STUDY OF THE CLAROMECÓ BASIN FROM GRAVITY, MAGNETIC AND GEOID UNDULATION CHARTS

Francisco RUIZ &Antonio INTROCASO

Boletín del Instituto de Fisiografía y Geología

Ruiz F. & Introcaso A., 2011. Study of the Claromecó Basin from gravity, magnetic and geoid undulation charts. *Boletín del Instituto de Fisiografía y Geología* **79-81**: 95-106. Rosario, 01-07-2011. ISSN 1666-115X.

Abstract.- In this work we analyze crustal characteristics of Claromecó intermontane basin using gravity and magnetic anomalies, and local geoid undulations. They are:
i) isostatic compensation (based on Airy hypothesis), related to stretching;
ii) old sediments filling the basin, covering more than 12 km, with a density contrast value of -100 kg m^{-3}, resulting to be well balanced by an antiroot filled with upper mantle materials.

A crustal model is proposed justifying both observed Bouguer anomalies and local geoid undulations. A chart of isobath contours is builded using a quadratic equation involving sediments' thickness and local geoid undulation. Magnetic basement depth Z_T and Curie point depth Z_B are obtained using spectral analysis on a total field magnetic anomaly chart. Results show that Z_T reaches a maximum value of 12 km, whereas Z_B attains a minimun value below the Claromecó basin. The basin puts aside two different depth domains of the Curie isothermal surface: at the southwestern zone of the Ventania ranges Z_B is about 25 km, while northeast of these mountains Z_B is about 30 km.

Key-words: Claromecó sedimentary basin; Potential fields; Isostasy; Crustal model.

Resúmen.- ***Estudio de la Cuenca Claromecó a partir de cartas de gravedad, magnetismo y ondulaciones del geoide.*** Sobre la base de anomalías de gravedad, anomalías magnéticas y ondulaciones del geoide local determinadas en la cuenca intermontana de Claromecó, se investigaron las siguientes características corticales:
i) existencia de compensación isostática basada en la hipótesis de Airy, lo cual se relaciona con estiramiento cortical;
ii) la presencia de más de 12 km de sedimentos antiguos rellenando la cuenca, con un contraste de densidad de -100 kg m^{-3}, bien balanceados por una antirraíz ocupada por materiales del manto superior.

El modelo cortical encontrado puede reproducir tanto las anomalías de Bouguer como las ondulaciones del geoide local observadas. Una ecuación cuadrática que relaciona espesores sedimentarios y ondulaciones locales del geoide, nos permite definir las isobatas de la cuenca. Sobre una carta de anomalías magnéticas de campo total se llevó a cabo análisis espectral para calcular profundidades al basamento magnético Z_T y al punto de Curie Z_B. Z_T llega a un valor máximo de 12 km, mientras que Z_B alcanza valores mínimos bajo la cuenca de Claromecó. Esta cuenca separa dos dominios de profundidad diferente en la superficie de la isoterma de Curie: en la zona sudoeste de las sierras de Ventania las Z_B están en los 25 km de profundidad, mientras que al noreste de estas montañas Z_B son del orden de los 30 km.

Palabras clave: Cuenca sedimentaria Claromecó; Campos potenciales; Isostasia; Modelo cortical.

Adresses of the authors:

F. Ruiz [fruiz@unsj-cuim.edu.ar]: *Instituto Geofísico Sismológico "Ing. Fernando Volponi", Universidad Nacional de San Juan, Meglioli 1160 (sur), 5400 Rivadavia, San Juan, Argentina.*
A. Introcaso: *Instituto de Física de Rosario, Universidad Nacional de Rosario and CONICET, Av. Pellegrini 250, 2000 Rosario, Argentina.*

Received: 17/03/2011; accepted: 10/05/2011

INTRODUCTION

It is well known that seismic and gravimetric methods usually produce reliable models to study sedimentary basins. In order to investigate the crustal structure of the Paleozoic Claromecó sedimentary Basin (Fig. 1), we have employed gravity, magnetic and geoid undulation charts, as well as some seismic interpretations (Kostadinoff & Prozzi 1998, Franke et al. 2002, Lesta & Sylwan 2005).

The *P*-wave velocities obtained from refraction tests on dense Paleozoic sedimentary rocks of this basin are very similar to the values determined for the underlying crystalline basement. The small differences make difficult to distinguish both units using seismic speeds exclusively (Zambrano 1974, Introcaso 1982, Ploszkiewicz 1999, Ramos & Kostadinoff 2005). This situation emphasizes the interest in using potential field methods to study the crust in this region.

In this work we build a local chart of geoid undulations for the basin. Turcotte & Schubert (2002) point out that geoid anomalies are not zero on isostatically compensated zones and they provide additional information on density versus depth distribution. These authors also note that isostatic mechanism can be inferred by comparing observed results with predictive ones (*e.g.* Airy-Pratt models). In fact, using traditional gravity methods together with local geoid anomalies, we attempt to define the isostatic compensation system and the crustal thickness for this area. By analysing magnetic anomalies we calculate depth values for the magnetic basement and Curie point depths for the region.

The intermontane Claromecó Basin has been previously studied using gravity data (Introcaso 1982, Kostadinoff & Font 1982, Ramos & Kostadinoff 2005), or gravity perturbations (Gil et al. 1995). Introcaso (1982) presented three alternative models obtained through the inversion of Bouguer anomalies along a NNE-SSW section near the coast. One of these models showed a maximum sedimentary thickness of about 10 km. Kostadinoff & Font (1982) and Gil et al. (1995) found maximum sedimentary thicknesses of 9 km. Lesta & Sylwan (2005), using 2D seismic studies, oil exploration wells and aeromagnetic data (unpublished information of hydrocarbon exploration) produced a profile in which they assume a crystalline basement depth of more than 10 km.

All previous models have shown very thick sedimentary sequences filling the basin, but they have considered only the sedimentary rocks filling it. In this work we present a more complete model and we also give an interpretation of the whole crustal structure on which the basin could have developed.

Our model shows: (1) the presence of an attenuated crust related to the antiroot thickness and the amount of sediments necessary for isostatic equilibrium, and (2) 12 km of Palaeozoic sediments (Tankard et al. 1996) which could partly be Neoproterozoic (Ramos & Kostadinoff 2005).

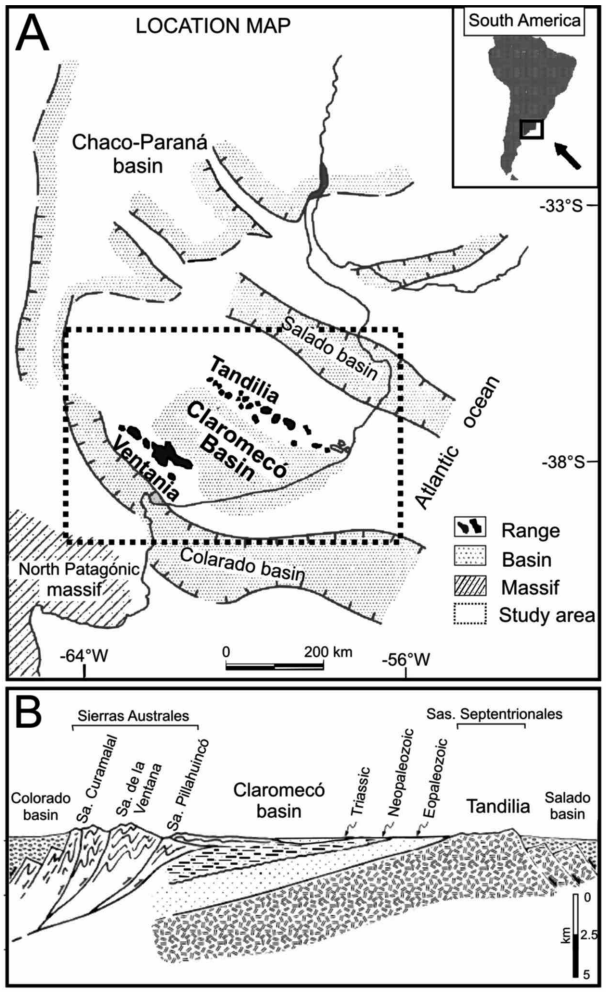

Figure 1. Location map. **A.** Geotectonic sketch map and location of the studied area (modified from Limarino et al. 1999). **B.** Schematic cross section of the Claromecó Basin (after Ramos 1999).

GEOLOGICAL SETTING

The Claromecó Basin (Ramos 1984) is located between Tandilia and Ventania ranges in the south of the Buenos Aires Province (Fig.1). Some authors have considered that it is an intermontane basin (López-Gamundi & Rosello 1992) or a back arc foreland basin (Lesta & Sylwan 2005). Claromecó Basin is asymmetric and has a NW-SE trending axis (Fig. 1). According to Lesta & Sylwan (2005) its onshore sector has a surface of about 50 000 km^2, although its offshore limits are uncertain. Its location can be approximated by zero gravity anomaly contours (Fig. 2B).

Ramos (1999a) has suggested that Claromecó Basin foundation is due to thrust loading during Devonian-Middle Permian (Chañic-Sanrafaelic tectonic phases). The Late Paleozoic Las Tunas Formation could be the result of synorogenic deposition (López-Gamundi et al. 1995). Sedimentary sequences extensively appear on both sides of the basin. The basin is mainly filled with Neopaleozoic sedimentites (Andreis et al. 1989), which crop out mainly in the Pillahuincó zone and slightly near the Tandilia hills edge (Fig. 1). It was also pointed out (Pucci 1995) that age, deformation and metamorphism of the rock units increase from east to west. Thus, it is possible that gentle deformed structures capable of trapping fluids could be present, east of the Ventania ranges (also known as Sierra de la Ventana), in the basin subsurface. This author also indicated that, west of the Tandilia hills, the basement is block faulted, thus having given rise to anticlinal structures which closures in Post-Precambrian sediments, so in the subsurface there could be traps for hydrocarbons (Lesta & Sylwan 2005).

According to Ramos (1984) the Sanrafaelic (Ventania Ranges) orogeny is a consequence of compressional tectonics that amalgamated Patagonia and Gondwana terranes. The Cape (South Africa) and Ventania Systems share documented common features (du Toit 1927, Tankard et al. 1996, Ramos 1999, 2008, Pankhurst et al. 2006), there is a growing consensus that the Ventania fold-and-thrust belt is the

continuation of the Cape fold belt and that the Claromecó foreland Basin is the western end of the Karoo Basin, both of them with a thickness exceeding 10 km.

Most of the present reconstructions of the Gondwana accept that its southwest margin consisted of a continuous clastic passive margin that extended from Ventania ranges to the Cape System (Pankhurst et al. 2006, Ramos 2008). An early stage of rifting affecting the Proterozoic basement was postulated by Rapela et al. (2007), based on geochemical characteristics and the age of some 531–524 Ma granites and rhyolites interpreted as a Cambrian rift and correlated with similar rocks in the conjugate margin of South Africa. Depocenters bounded by northwest-trending normal faults have been observed in the seismic lines of the Claromecó Basin, perpendicular to the margin and correlated with this rifting (Ramos & Kostadinoff 2005). Sequences of platformal orthoquartzites (Middle-Late Cambrian and Devonian times) of the Curamalal and Ventana Groups were unconformably deposited on metamorphic basement. Paleocurrent analyses of these mature sequences indicate a provenance from the northeast. A molasse sequence exposed east of the thrust front, the Pillahuincó Group, unconformably overlying the Devonian quartzites and associated with glacial deposits in the lower section has a Late Carboniferous to Early Permian age. These immature sandstones with volcanic clasts have a southwestern provenance. The changes between the stable clastic platform and these immature deposits indicate an important modification in the transport direction from NE to SW in the base, to SW to the NE in the upper section; an increase of instability in the basin, and the existence of a positive relief to the south (López-Gamundi & Rossello 1992).

The Ventania fold-and-thrust belt is characterized by isoclinal folds associated with a high strain in the orthoquartzites (Ramos 2008). The southwestern part of the belt, where the basement is exposed, has evidence of thrusts associated with low grade metamorphism constraining the deformation between Lower and Middle Permian. As a result of the thrust stacking, the Claromecó foreland Basin was formed by flexural loading of the Gondwana margin with a foredeep more than 10 km in thickness. Ramos (2008) proposed a southward subduction of the Gondwana clastic passive margin stopped after the Carboniferous. First contact between Patagonia and Gondwana may have started during the Carboniferous, but collision, deformation and uplift took place in Early Permian times. The compressive stress regime lasted in this sector of South America to the Late Permian, when a generalized extension took place.

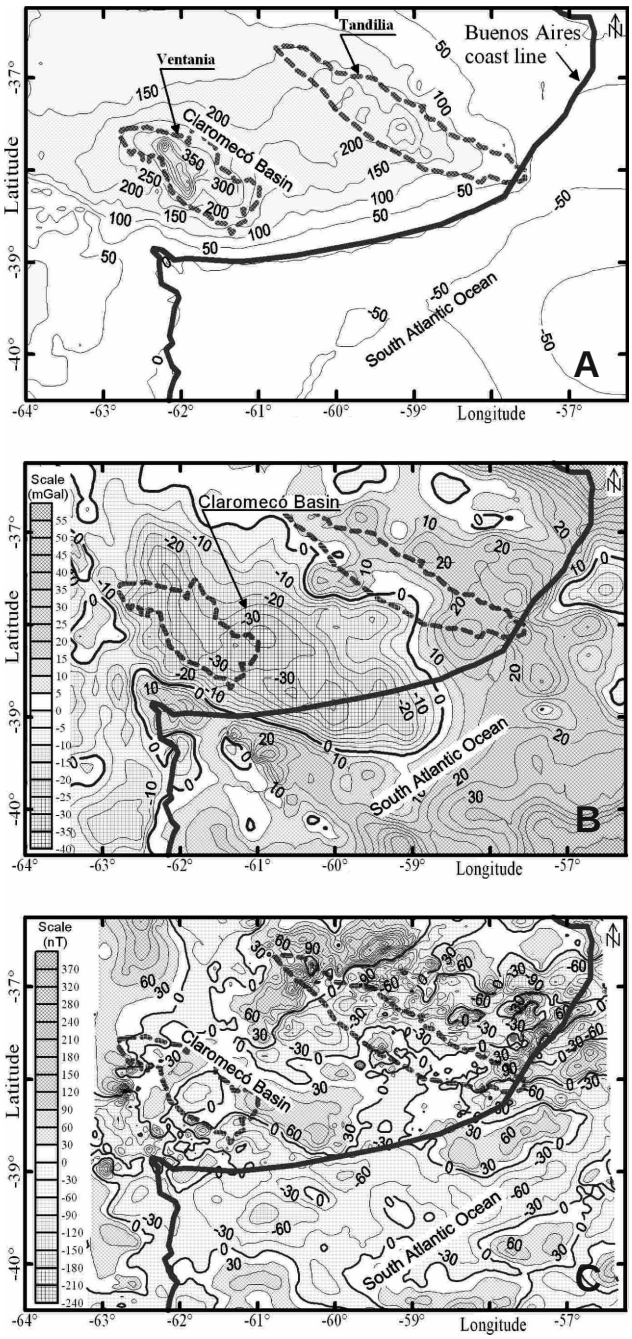

Figure 2. A. Topographic map (contour interval 50 m). **B.** Bouguer anomaly map (contour interval 10 mGal). **C.** Total magnetic anomaly map (contour interval 50 nT). Gravity data from Instituto de Física de Rosario, Instituto Geográfico Militar Argentino, Universidad de La Plata, Universidad de Buenos Aires and University of Leeds. Magnetic data from Instituto Antártico Argentino.

CRUSTAL MODEL

In order to design a crustal model we have determined: (1) local geoid undulations (N_l), (2) crustal thicknesses below the Claromecó Basin, (3) Curie point depths, (4) sediments, crust and upper mantle densities, and (5) the isostatic state of the Claromecó Basin. An initial crustal model is thus proposed, and (6) double inversion of gravity anomalies (g) and local geoid undulations (N_l) is applied for improving the model.

Calculation of local geoid undulations

Perdomo & Del Cogliano (1999) have presented a geoid undulations chart of the Buenos Aires Province (Fig. 3). They have calculated geoid undulations (N) from ellipsoidal and orthometric heights ($N \approx h - H$) measured in a regular geodetic network.

The arrows in Fig. 3 indicate the contour deformation tendencies over Salado Basin (S), Tandilia high (T) and Claromecó Basin (C). Undulation contours are interrupted near the coast suggesting an offshore continuation of the basin. Fig. 2B-2A corroborate this possible continuation of the basin on the continental platform. Thus, we have extended the geoid chart into the oceanic zone using the global model EGM2008 (Pavlis et al. 2008) and then we have eliminated Tandilia and Ventania ranges topo-isostatic effects of topographic masses and the corresponding compensation roots (Forsberg 1985).

For the obtention of the local geoid undulations (N_l) on

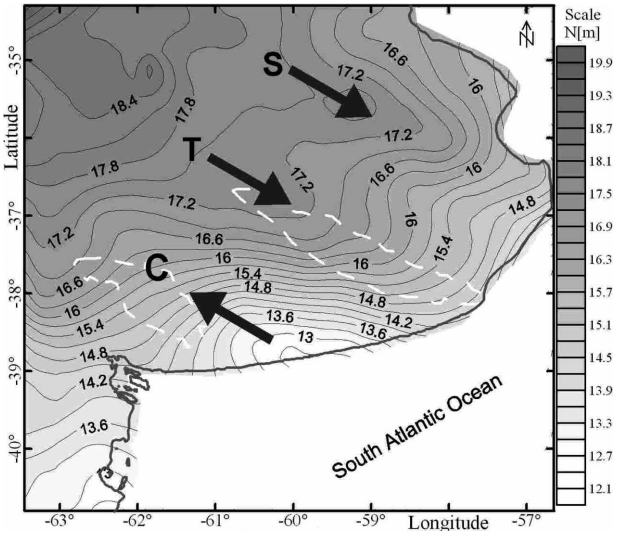

Figure 3. Geoid undulation map '*N* ' (*N* ≈ *h* - *H*) based on Perdomo & Del Cogliano (1999), contour interval 0.3 m. Arrows indicate the deformation tendencies of the contours. Salado (S) and Tandilia (T) trends to the SE; Claromecó (C) trend to the NW.

Claromecó Basin, we have removed wavelengths (λ) larger than 500 km (studied geological structure width) applying a band pass filter (40 ≤ λ ≤ 500 km). Results are presented in Figure 4B.

Turcotte and Schubert (2002) have pointed out that geoid anomalies are not zero on isostatically compensated zones and they provide additional information on density versus depth distribution. On the Claromecó Basin negative N_1 values have been found. In contrast, positive geoid undulations were found on the adjacent Salado and Colorado Cretaceous Basins. Introcaso (2003) has found an excess of isostatic compensation masses in the lower crust for the two latter sedimentary basins, providing arguments for the importance of the study of the Claromecó Basin deep structure.

Crustal thickness

There is no available published information on crustal thickness values for the Claromecó Basin. Franke et al. (2002) have published an integrated interpretation of multichannel reflection seismic data and a wide-angle E-W trending offshore refraction seismic line, at 40°S latitude, along the Colorado Basin axis. Results of seismic reflection measurements (Kostadinoff & Prozzi 1998, Ramos & Kostadinoff 2005) furnish some information on the sedimentary thickness. We have used the seismically derived depths published in those papers to constrain depths to crustal interfaces calculated from potential fields in the Claromecó Basin region.

Gravity anomalies 'g' (terrestrial data from the Instituto de Física de Rosario, 2001, oceanic data from GETECH, Leeds University 1995; Fig. 2B) and total magnetic field anomalies 'T' (Ghidella et al. 2002; fig. 2C) have been used to calculate sedimentary thickness, crustal depths and the geometry of regional geological structures. The following techniques have been used: (1) Fourier analysis of 'g' and 'T'; (2) 3D Euler deconvolutions of 'g' and 'T'; (3) Werner deconvolutions of 'g' and 'T'.

Fourier analysis: Crustal thickness has been calculated from Bouguer gravity anomalies and total magnetic field anomalies.

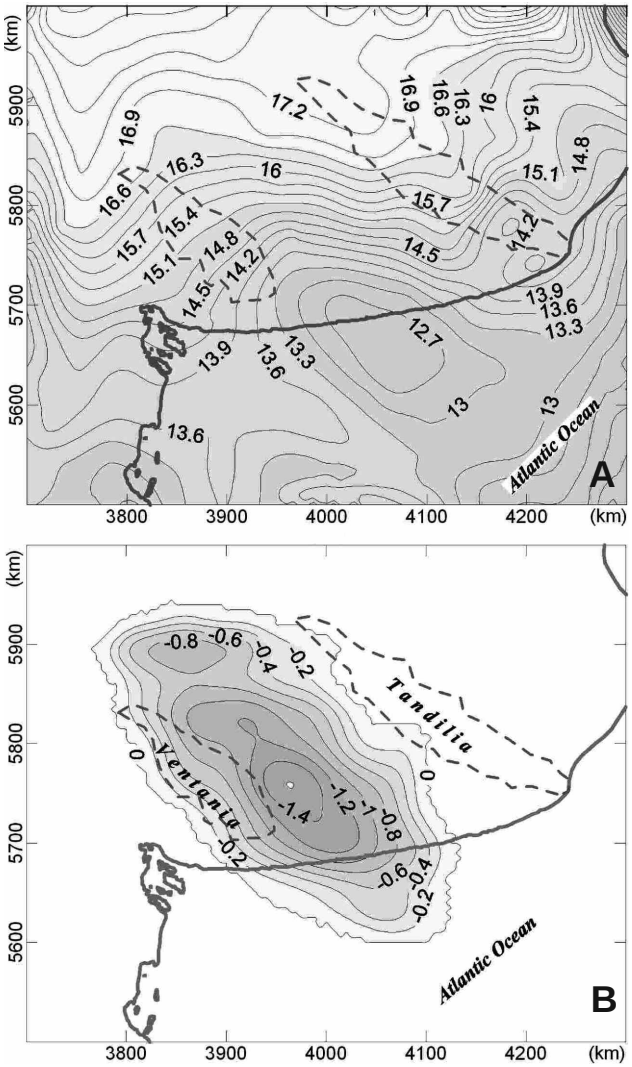

Figure 4. A. *N* (Perdomo & Del Cogliano 1999) extended into the ocean (EGM2008; Pavlis et al. 2008) and isostatically corrected by elevation above the geoid (mixed continental and oceanic area using equivalent sea/rock root conversion); contour interval 0.3 m; **B.** Local geoid undulation 'N_1' in meters, obtained after filtering (band pass filter 40 ≤ λ ≤ 500 km); contour interval 0.2 m.

The depth of anomalous bodies (*N* levels of concentration of source material at a depth z_i) has been obtained in the frequency domain from a logarithmic graph of the radially averaged power spectrum |*G*(k)| versus wave number (*k*) of the observed potential field (Spector & Grant 1970, Blakely 1995):

$$|G(k)| = \sum_{i=1}^{N} A_i \, e^{(-z_i|k|)} + \overline{WN} \qquad \text{(Eq. 1)}$$

where A_i depends on the anomalous sources magnitudes and *WN* corresponds to the white noise spectrum.

The long wavelengths of the gravity field have been analyzed in square windows 200 km wide, being displaced by steps of 50 km covering the area which extends from 35° to 42° S latitudes and from 56° to 64° W longitudes. From the lowest wave numbers of the power-density spectra, mean depths (to the base of the crust) have been calculated. The results are shown in Fig. 5A. Near the Claromecó Basin, crustal thicknesses of (36 ± 2) km have been obtained on land, and depths of (32 ± 2) km have been found in the offshore portion of the basin. Lowest depths to the Moho, (30 ± 2) km, have been

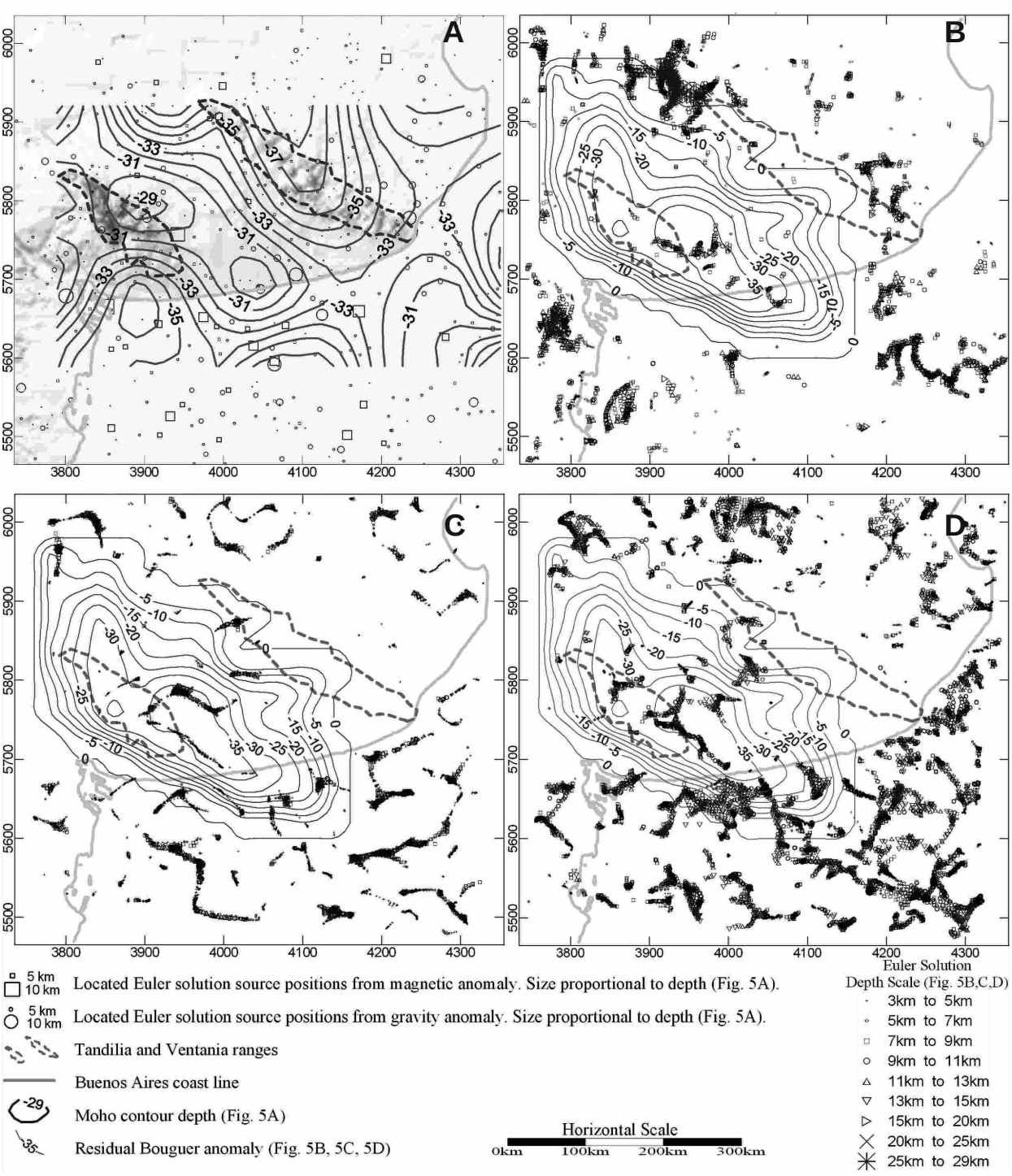

Figure 5. A. Shaded relief map of Buenos Aires Province with superimposed Moho depths obtained from spectral analysis (contour interval 1 km) and located 3D Euler solutions from magnetic data (squares) and from gravity data (circles), size proportional to depth (see references). **B.** Standard Euler solutions structural index SI = 1 from gravity data. **C.** Standard Euler solutions SI = 0 from magnetic data. **D.** Standard Euler solutions SI = 0.5 from magnetic data. In **B**, **C** and **D** residual gravity anomaly, obtained after applying a band pass filter ($20 \leq \lambda \leq 500$ km), contour interval 5 mGal.

obtained below the basin.

In the next section a spectral analysis of magnetic field anomalies has been carried out for determining the Claromecó Basin magnetic basement thickness (Fig. 7).

3D Euler deconvolutions of 'g' and 'T': 3D Standard Euler deconvolutions (SED) and Located Euler deconvolutons (LED) have been applied to gravity and magnetic data using Oasis Montaj 6.2 software (Geosoft). The apparent depth to the magnetic (or gravimetric) source has been automatically derived from Euler's homogeneity equation:

$$(x-x_0)\frac{\partial T}{\partial x}+(y-y_0)\frac{\partial T}{\partial y}+(z-z_0)\frac{\partial T}{\partial z}=N(B-T) \qquad \text{(Eq. 2)}$$

where (x_0, y_0, z_0) is the position of the magnetic (or gravimetric) source whose field (T) is detected at (x, y, z); B is the regional field ('g' or 'T'); N is the fall-off rate of the potential field and may be interpreted as the structural index (SI).

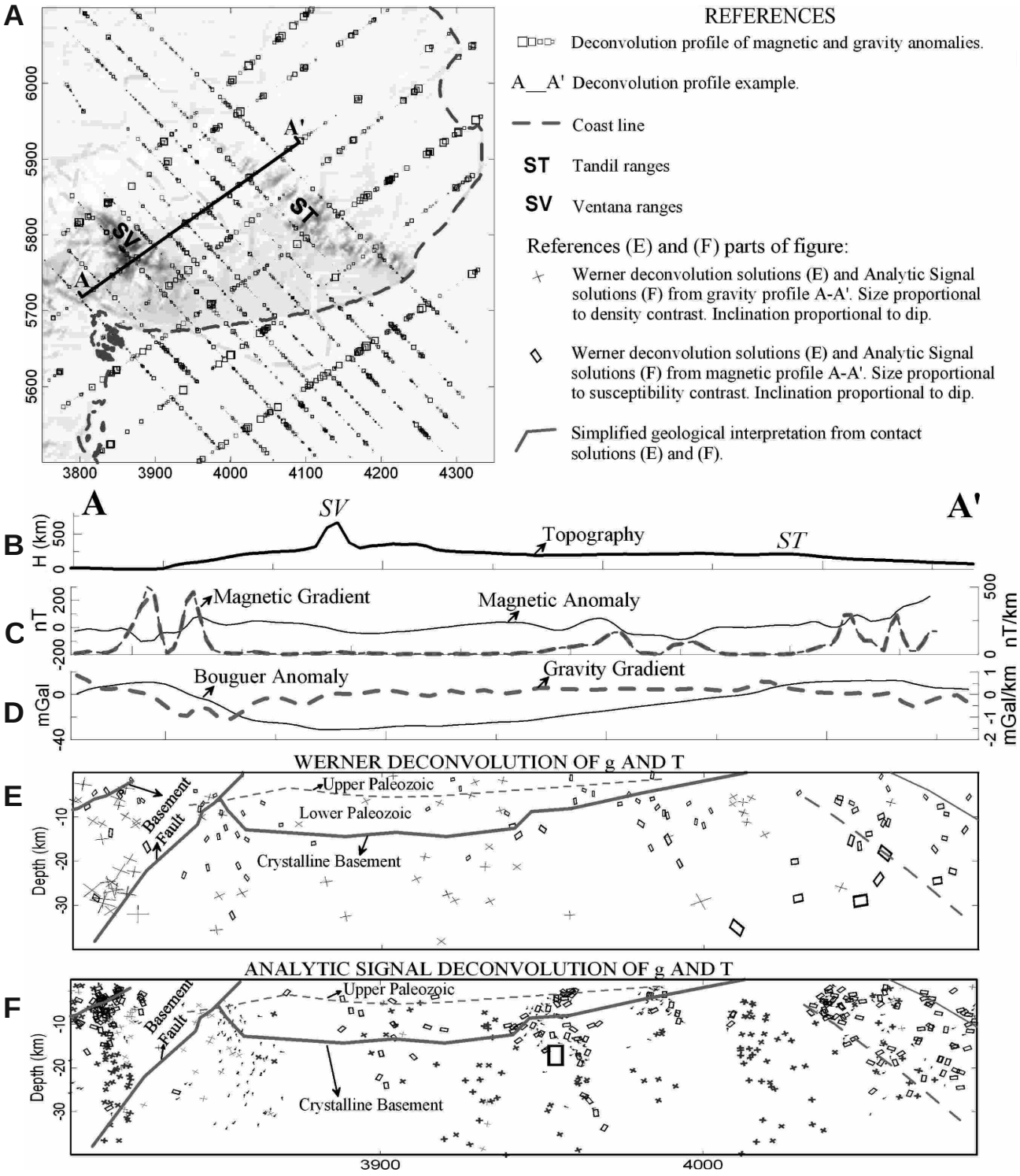

Figure 6. A. Werner and Analytic Signal deconvolutions profiles location (squares: contact solutions size proportional to depth). Deconvolutions cross section example (A-A'): Topographic profile **(B)**; total magnetic anomaly and magnetic gradient **(C)**. **D.** Bouguer anomaly and gravity gradient. **E.** Werner deconvolutions from gravity and magnetic data. **F.** Analytic Signal deconvolutions from gravity and magnetic data. In **(E)** and **(F)** interpretations of the principal geological structures.

This process relates the anomaly and its gradient components to the location of the source of an anomaly, with the degree of homogeneity expressed as a structural index (Thompson 1982).

The method consists of setting an appropriate SI value and using a least-squares inversion to solve Eq. 2 for optimum (x_0, y_0, z_0) and B (Reid et al. 1990). A square window size must be specified in the gridded 'T' for to be used in the inversion at each selected solution location and then run over all the anomalies map. In SED the window should be large enough to include each solution anomaly of interest. Using LED the window size is automatically calculated using the Analytic Signal Wavelength (Nabighian 1972). Examples of appropriate models for structural index values are: a) SI = 0 to 0.5; contact

(depth to the border layer with density or susceptibility changes) and step (depth to fault step); b) SI = 1 to 1.5; dipping step, sill, dyke, cylinder and pipe; c) SI = 2 to 3; cylinder and sphere. The method allows to locate or to outline confined sources and provides a series of depth-labeled Euler trends marking edges and faults with high precision (Reid et al. 1990). The correct index for any given feature is chosen as the one giving the tightest solutions cluster.

In the present paper the regional geological structures (top of the basement geometry and deep basement faults) are described by using SED with low structural index in windows sized 30 to 45 km on 'g' and 'T' anomalies. The SED results are plotted in Fig. 5 together with the residual Bouguer anomalies obtained by a band pass filter of 50 km $\leq \lambda \leq$ 500 km. The minimum residual anomalies can be associated with the maximum sedimentary thicknesses in the Claromecó Basin.

The northwest-southeast striking basin axis (-35 mGal Bouguer anomaly) is clearly indicated towards the east zone of Ventania from 'T' with SI = 0 (contacts, Fig. 5C) and 0.5 (steps, Fig. 5D) and from 'g' anomalies with SI = 1 (dipping steps, Fig. 5B). This axis indicates maximum depths to basement from 8 km at grid node (3880, 5800), increasing to 11 and 12 km between nodes (3910, 5770) and (3940,5740); 9 and 10 km at (4040, 5675) and gradually diminishing to 5 km at (4090, 5640) where ends this 400 km long alignement of contacts. This alignment continues offshore in the Colorado Basin domain with index of 0.5 and can be interpreted as a regional basement fault.

North of Ventania the contacts maximum depths reach 7 to 8 km at grid node (3870, 5835) and 15 km northwards the solutions cluster ends. This means that the potential fields do not include significant gradients which could indicate lack of structural complexity.

In accordance with 12 to 14 km maximum depths at (3930, 5780), contact nests 200 km long (SI = 0 and 0.5) align along a west-east strike. Their depth gradually diminishes eastwards to 7 km at (4020, 5770). Maximum depth solutions cluster agrees with the -35 mGal gravity minimum (Fig. 5B-D). At the northeastern of this structure, depth values steeply diminish, thus indicating an elevation of the basement top. These results are also based on Located Euler Deconvolutions carried out on 'g' and 'T' values (Fig. 5A) where maximum sedimentary thicknesses were placed at the axis of the basin.

Werner and Analytic Signal deconvolutions of 'g' and 'T': Werner deconvolutions (WD) and Analytic Signal depth solutions (ASD) were carried out on the magnetic and gravity fields along 18 profiles (Fig. 6A), 11 of them running from NW to SE and the other 7 running from SW to NE, using Pdepth Oasis Montaj 6.2 (Geosoft) module.

The WD (Hartman et al. 1971, Phillips 1997) and ASD (Nabighian 1972, Phillips 1997) methods for magnetic (or gravity) profiles have been widely used as part of an automated interpretation routine system. Assuming hypothetical source geometry, the Werner-based Deconvolution of the recorded field yields to a two-dimensional geologic source distribution and an associated magnetic parameter distribution: Werner's (or SA) depths, horizontal locations, dip angles, and magnetic susceptibility contrasts (Phillips 1997).

The Werner observed field solution is a good indicator of a thin-dike body. The Werner horizontal gradient solution is a good indicator of the edge of a thick interface body (contact). The use of these two extreme types of solutions lead to a close approximation to depth estimation and reveal the geometry of different magnetic (or gravimetric) bodies including those lying somewhere between a thin dike and the edge of a thick

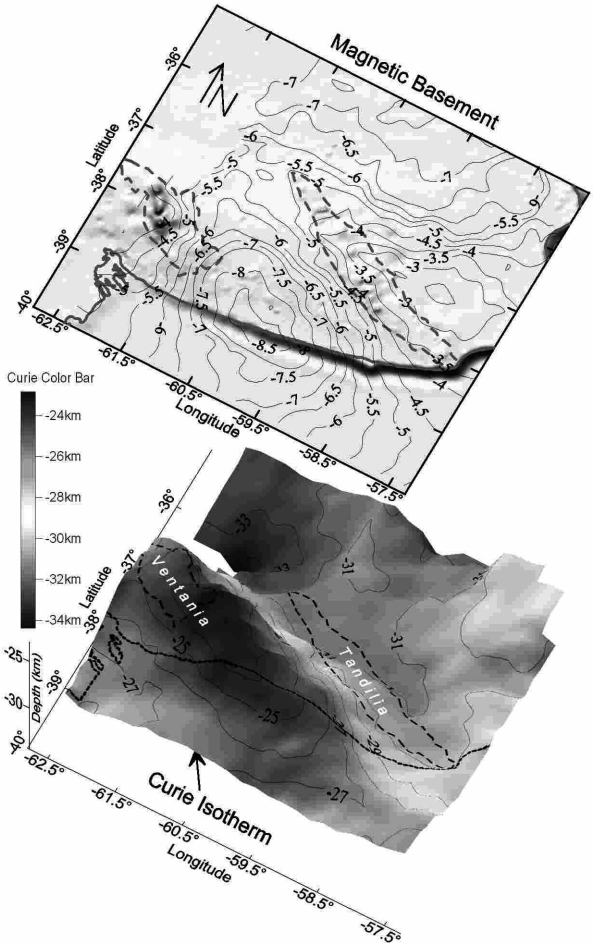

Figure 7. Spectral analysis from magnetic data. Above: magnetic basement mean depth (Z_t); contour interval 0.5 km. Below: Curie isotherm depth (Z_b); contour interval 1 km.

interface (Ku & Sharp 1983). Contact solutions on all the profiles have been analyzed. Claromecó Basin boundaries are clearly identified and regional structures have been enhanced, especially the basement depth (see section A-A' taken as an example in Fig. 6).

Sweeping deconvolution operator along each field profile, different series of solutions can be estimated. Depths are indicated by crosses (from g) and rectangles (from *T*) respectively with the same dip angles of each solution (dip angle of the body interface), and susceptibility (or density) contrasts proportional to the symbol size (Fig. 6E-F).

Basement outcrops located westwards Ventania ranges make up the western limit of the basin, also defined by the southwest dipping basement fault interpreted in Fig. 6E-F. On the eastern border of the profile we interpret two faults dipping to the east in the Tandilia basement.

Maximum sedimentary depths have been analyzed by separating less than 0.002 emu susceptibilities contact solutions. These solutions are located below and eastwards Ventania ranges and the thickness thereby obtained gradually diminish eastwards and wedge out to the west of the Tandilia Hills. Below Ventania ranges the contact solutions found indicate depths over 12 km.

Subhorizontal top of Analytic Signal solutions are interpreted as Neopaleozoic sediment depths according to Lesta and Sylwan (2005).

A large concentration of contact solutions at progressive 3950 km are interpreted as a structural step in the basement (Fig. 6E-F).

Curie Point Depth

Upper and lower boundaries of the magnetized crust have been obtained from spectral analysis of magnetic anomalies. We have assumed lowest depths obtained for the magnetized crust as corresponding to Curie point depths (Blakely 1995). Frost & Shive (1986) have shown that crustal magnetic sources must lay at a depth in which temperature is high enough for the magnetite to become paramagnetic, *i.e.*, 578ºC. Deviation from the Curie point temperature indicates distortion of the thermal structure of the lithosphere (Ruiz & Introcaso 2004).

We have used a method (Ruiz & Introcaso 2004) modified from Tanaka et al. (1999). Upper boundary (Z_t) and the centroid (Z_c) of the magnetic basement (crustal magnetic plate) have been determined from the total-field anomaly power-density spectra. The bottom of the plate (Curie point depth) has been determined as: $Z_b = 2Z_c - Z_t$, where Z_t can be interpreted as the mean upper boundary of the crystalline basement. It has been determined by using the relationship $\ln[\Phi_{\Delta T}(k)^{1/2}] = \ln A - |k| Z_t$. Besides, the relationship $\ln\{[\Phi_{\Delta T}(k)^{1/2}]/|k|\} = \ln B - |k| Z_c$, has been used to determinate the centroid depth $|\Phi_{\Delta T(k)}|$ is the power-density spectra of magnetic anomalies; k is the wave number; A and B are constants related to magnetic masses. Z_t and Z_c are estimated by fitting a linear function to the high-wave number and low-wave number parts of the respective logarithms of radially averaged spectrum.

The spectral analysis has been carried out in 300 square windows 175 km side. Steps of displacement are 25 km along the longitude and 50 km along the latitude, covering the whole studied area (which extends from 34°30' S to 40°30' S and from 56°45 'W to 63°25' W). Calculated Z_t and Z_b have been referred to each window centre. Fig. 7 shows mean depths to magnetic basement, reaching 9 km at the south of Ventania.

Results are interesting as they show Curie isothermal significant changes on both sides of the Claromecó Basin axis (Fig. 7). Z_b depths at the north of the basin are about (31 ± 2) km and below maximum sedimentary thickness Z_b reaches 23 km depth, increasing to 27 km at the basin southwest.

In summary, from the above analysis, we can say that the Claromecó Basin has more than 10 km of sedimentary loading and is set on an attenuated crust with a shallower Curie isotherm below Ventania ranges.

Crust and Upper Mantle densities

In the selection of densities we have taken into account that Zambrano (1974), based on YPF Petroleum Company refraction seismic data, has informed that compression wave velocities *V*p of Paleozoic sediments in the basin are very similar to those of the crystalline basement. On the other hand, Zambrano (1974) has concluded that the sedimentary load is very thick. Introcaso (1982) has pointed out that old sediments have suffered strong compression. It seems that these sediments are very compact and dense because of this compression, with an incipient metamorphism. This fact justifies the high velocities *V*p found which makes hard to separate sediments from the crystalline basement on the sole basis of seismic velocities. On the other side, the gravimetrical method allows us to justify Bouguer anomalies of -30 mGal from a combination of low negative density contrasts between sediments and crystalline basement, as it was suggested by

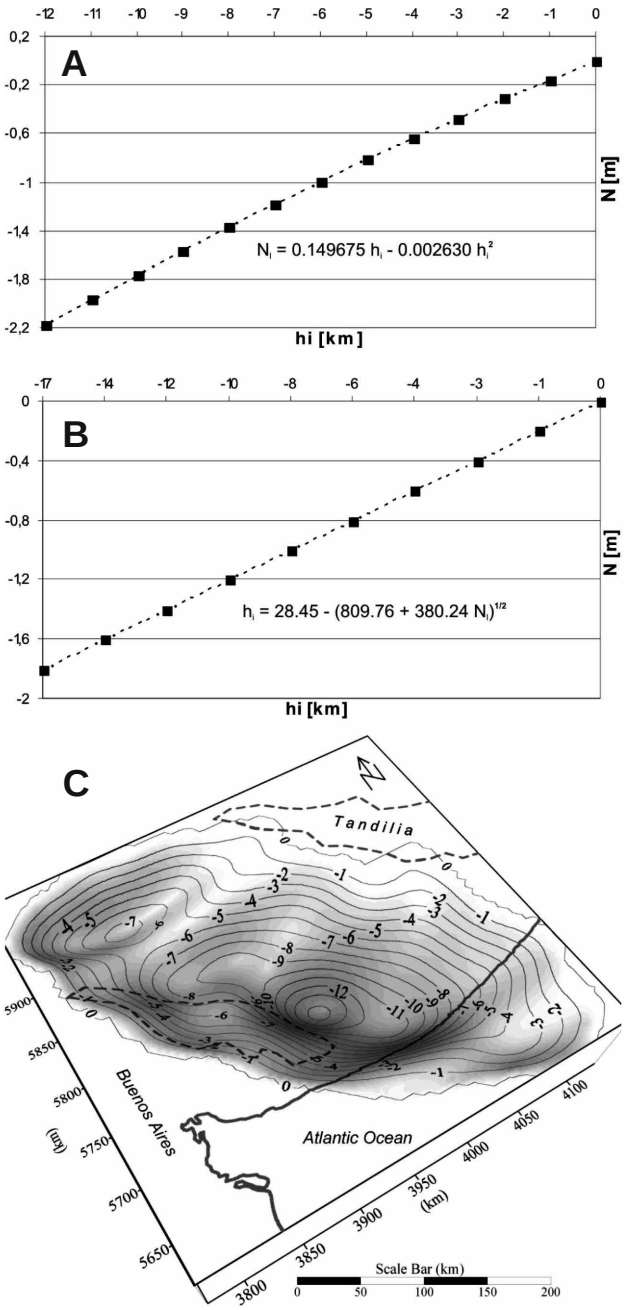

Figure 8. Geoid undulation due to a sedimentary basin isostatically compensated in the Airy system. Density contrasts: $\Delta\sigma_s$ = -100 kg m^{-3} and $\Delta\sigma_m$ = 400 kg m^{-3}, normal crustal thickness 35 km, antiroot R = 0.25 h_i, where h_i is the sedimentary thickness of the basin. **A:** Initial crustal model Nl = 0,149675 h_i-0,00263h_i^2; **B:** Quadratic expression h_i = -8,45 + (809.76+380.24 Nl)$^{1/2}$; **C:** Sedimentary thickness of a basin isostatically compensated obtained from **(B)** and Fig. 4B.

seismic results and by the high sedimentary thicknesses.

Using the gravimetric method, considered appropriated to obtain preliminary interpretations, Introcaso (1982) has found a thickness of (10 ± 4) km assuming density contrasts of $\Delta\sigma_s$ = -(70 ± 30) kg m^{-3}; Kostadinoff & Font (1982) have found 8 km of sedimentary thickness assuming a density contrast of $\Delta\sigma_s = \sigma_S - \sigma_C$ = -100 kg m^{-3} between sediments (σ_s) and crystalline basement (σ_c).

It is well known that there exists a relationship between

compression wave velocities V_P and densities σ (Woollard 1959, Brocher 2005). From recent seismic reflection and airborne gravity surveys and well studies, Lesta & Sylwan (2005) have found more than 10 km sedimentary thickness, indirectly confirming the density contrast previously assumed. These results have been maintained on strict confidentiality by petroleum exploration companies.

It is important to point out that all the models mentioned above are significantly incomplete since they only take into account the highest part of the upper crust. The model we present in this work involves the whole crust, adding another density contrast: lower crust-upper mantle. Lacking deep seismic data (Moho and subMoho) we have assumed $\Delta\sigma_m = \sigma_m - \sigma_{lc} = +400$ kg m^{-3} following studies in nearby regions: (i) Salado Basin (Introcaso & Ramos 1984, Introcaso et al. 2002) and (ii) Colorado Basin (Introcaso 2003). Note that this density contrast is positive because lower crustal attenuation implies materials ascend from lithospheric mantle into the crustal antiroot.

According to the results obtained in the present study we assume: (1) the crust has been attenuated by extensional processes; (2) density contrasts are -100 kg m^{-3} (top of the upper crust-infill sediments) and +400 kg m^{-3} (antiroot in lower crust). Using these data we analyze: (i) isostatic state of the basin; (ii) the possibility of quickly obtaining the geometry of the basin (basement isobaths) in view of its isostatic compensation; Haxby and Turcotte (1978) formulas can be employed; (iii) crustal model obtained by double inversion.

Isostatic state of the basin

It has been noted above that the Claromecó Basin is emplaced on an attenuated crust. If there are isostatic equilibrium at crust level, the mass deficit produced by sedimentary load m_s should be balanced by the mass excess of the upper mantle m_m lodged in the antiroot. In this case:

$$\left|-m_s\right| = m_m \qquad \text{(Eq. 3)}$$

The isostatic anomaly *AI* is obtained by correcting Bouguer anomaly *AB* by the gravity effect originated by sediments C_s; then it is necessary to make the correction corresponding to gravity effect of a hydrostatically compensated antiroot model C_m (Introcaso 1993). Then

$$AI = AB + C_S - C_m \qquad \text{(Eq. 4)}$$

C_s can be computed if density contrast (in this case +100 kg m^{-3}) and basin geometry are known. In former publications the basin limits were established by Tandilia and Ventania, but the subsurface information was insufficient. Although gravity maps (Fig. 2B) suggest its continuation into the continental platform, NW and SE borders were not well defined (Introcaso 1982, Kostadinoff & Font 1982, Ramos 1984, López-Gamundi & Rosello 1992, Pucci 1995, Lesta & Sylwan 2005, Ramos 2008).

The Local geoid *Nl* map presented in Fig. 4B can be used to characterize the whole basin. Haxby & Turcotte (1978) pointed out that geoid anomalies could have negative values on isostatically compensated basins (Airy or Pratt models). Thus we have started assuming isostatic balance for the initial model. Simultaneous work with *AB* and N_l is useful for the analysis of masses balance.

We have used Turcotte & Schubert (2002) models to calculate geoid undulations N_l in Pratt and Airy systems.

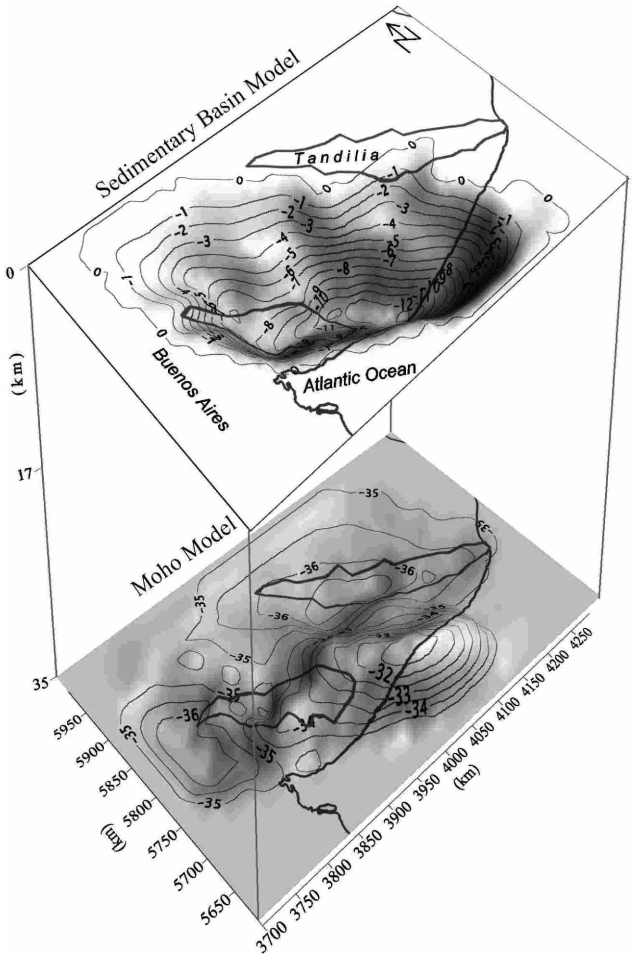

Figure 9. Crustal 3-D gravity-potential model obtained by double inversion. Sedimentary basin model (upper part) in km with root below the ranges and antiroot below the Claromecó Basin (lower part). Inversion model calculated in the Airy system in isostatic equilibrium (see text); density contrasts $\Delta\sigma_s = -100$ kg m^{-3} and $\Delta\sigma_m = 400$ kg m^{-3}.

According to crustal attenuation found by stretching, we have adopted the Airy system assuming 35 km crustal thickness (before stretching) and differential densities –100 kg m^{-3} (sediments-basement) and +400 kg m^{-3} (upper mantle-lower crust density). Antiroot thickness is $R = (\sigma_c - \sigma_s/\sigma_m - \sigma_{lc})h_i = 0.25h_i$, where h_i is the sedimentary thickness of the basin (unknown variable). With these values, Turcotte & Schubert (2002) expressions provide (see Fig. 8A and 8B):

$$Nl = 0.149675\,h_i - 0.002630\,h_i^2 \qquad \text{(Eq. 5)}$$

$$h_i = 28.45 - \left(809.76 + 380.24\,Nl\right)^{1/2} \qquad \text{(Eq. 6)}$$

Dipolar expressions used have a good performance if the analyzed structure width is much smaller than the Earth radius (Doin et al. 1996).

Geoid undulations shown in Fig. 4B used in Eq. 6 allowed us to obtain the basement isobaths map h_i shown in Fig. 8C. Maximum sedimentary thickness reaches 12 km. These values agree with the depths to basement obtained from spectral analysis, 3D Euler deconvolutions and Werner and Analytic Signal deconvolutions in the present paper.

Double inversion model

In order to validate the isostatic model presented in Fig. 8C, we have carried out a double inversion model from Bouguer anomalies and geoid undulations of the crust in the basin region. The model calculated by direct method from an initial crustal compensated model (Fig. 8C) has been compared with the observed values of gravity anomaly *AB* and geoid undulations N_1 and modeled by trial and error. Computations were made following gravity and geoid expressions of Guspí et al. (1987), Guspí (1999), Introcaso (1999), Guspí et al. (2004) and Introcaso & Crovetto (2005). In the modeling process, depths to the basement values calculated on crustal thickness (see Crustal thickness above) were incorporated to make the model anomalies fit to the observed values of *AB* and N_1.

Double inversion model (Fig. 9) reveals both the basin geometry and the Moho geometry. Crustal thickness below the basin reaches 32 km to the Southeast, and theoretical root below Tandil ranges reaches 37 km. This model shows reasonable correlation with the Moho depths calculated from spectral analysis.

Fig. 10 exhibits negligible isostatic anomalies over the basin, thus a reasonable masses balance in the basin region could be inferred.

It is worth to note that considering local geoid values and Bouguer anomalies for the obtention of crustal features and isostatic balance state, the consistency of the model is reinforced.

If direct faults are assumed to have existed previous to the sedimentation (Cobbold et al. 1986, Ramos 2008), crustal attenuation (shown in this work) and sedimentary load increment produced by tectonic stacking (Jordan 1981, Ramos 2008), a series of sedimentary and subsidence pulses can be generated (Introcaso 1980, Introcaso & Ramos 1984), converging to:

$$H = h\left(1-\frac{\sigma_s}{\sigma_m}\right)^{-1} \qquad \text{(Eq. 7)}$$

using stretching $\beta = 1.7$. In Eq. 7, H is the modern maximum sedimentary thickness (≈ 12 km); σ_s and σ_m are sediment and upper mantle densities (2570 kg m^{-3} and 3300 kg m^{-3}, respectively), and h is the initial graben infill thickness. With these values it is obtained 2.6 km for h and 35 - 2.6 - (35/β) = 12 km for the antiroot R.

Assuming a hypothetical horizontal spinning axis located at the middle of the crust (Fig. 9) and rotating 180° the crustal model, we can roughly obtain: (a) the upper boundary of the basement in the upper crust, and (b) Moho discontinuity in the lower crust. Both discontinuities, (a) and (b), characterize the crustal thickness previous to the sedimentation.

DISCUSSION

Few geophysical interpretations concerning the Claromecó Basin have been published, most of which cover only parts of the basin area. In recent years Oil Industry has carried out some exploration, but the results obtained are kept hidden.

In the present work, the authors have used results of the potential fields observed to tentatively solve some geophysical and geologic problems in this basin.

The geometry of the Claromecó Basin can be analyzed from the residual Bouguer anomaly chart (Fig. 5). Largest sedimentary thicknesses are generally correlated with gravimetric minima. Local geoid undulations calculated (Fig. 4) have given minimal values agreeing with less dense rocks (Fig. 8C).

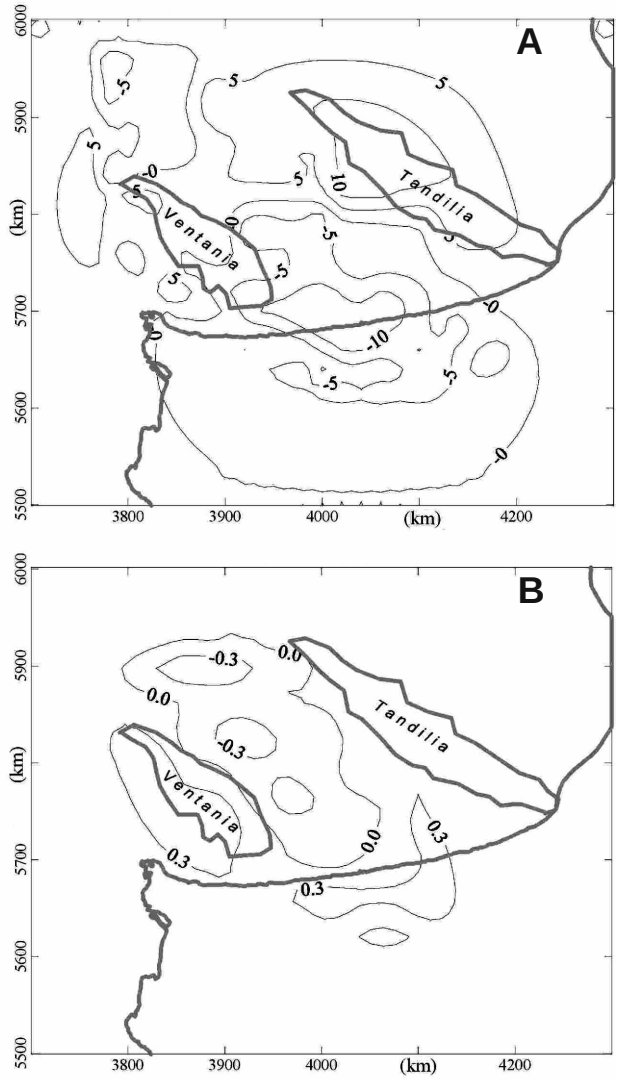

Figure 10. A. Isostatic anomaly from 3D crustal model (expression: $AI = AB + C_S - C_m$). **B.** The same as in A but with local geoid undulations, N_1 (Fig. 4B) minus geoid effects of the crustal model (Fig. 9).

The present authors calculations indicate that the maximum depths to the crystalline basement are about 12 km. Moreover, the largest sedimentary thicknesses are located beneath the Ventania ranges, gradually thinning eastwards. Then they wedge out at the western margin of the Tandilia hills (Fig. 6).

A regional fault associated with the Ventania axis has been interpreted. This fault surface dips SW and affects the whole crust (Figs. 5 and 6). The fault zone, 50 km wide, extends along 600 km. In the eastern area of the basin the crustal structures tend to dip NE (Fig. 6E-F).

Euler deconvolutions with low structural indices have given signs of discontinuities, especially in the crystalline basement (Fig. 5), also showing depth of this basement, indicating its main structures: faults and steps (Fig. 5B and 5D) and discontinuities in the basement (Fig. 5C).

The previously analyzed indicators have given information on the middle and upper crust. Nevertheless, the local geoid undulations, analyzed according to Turcotte and Schubert (2002), point out the existence of isostatic compensation in Airy's hypothesis, and a consequent attenuated crust beneath

the basin. This approach does not agree with the foreland model, which is the generally accepted as a geological model to explain the development of the Claromecó Basin (Ramos 1984, 1999a), unless crustal thinning could be a feature that has not been completely erased by the superposition of successive tectonic events during the evolution of the basin.

Respect to the lower crust, long wavelengths of gravimetric and magnetic anomalies have been analyzed. Spectral analysis on the gravimetric data indicates a crustal attenuation beneath the basin (Fig. 5A). The depth to the Curie isotherm is lower also under the highest sedimentary thicknesses of the basin.

A robust cortical model representing the entire crust could be proposed by inverting simultaneously Bouguer anomalies and local geoid undulations. In our model, calculated sedimentary thickness and the antiroot in Airy System (Fig. 9) are isostatically balanced. Sedimentary depths in this model are consistent with those calculated with Euler and Werner deconvolutions.

Moho discontinuity depth obtained by spectral analysis is also consistent with the model (Fig. 5A). Differences were found in the NE sector of Ventania, probably due to the lack of gravimetric data.

Considering a stretching mechanism to explain the development of Claromecó Basin, Eq. 6 can be used to obtain sedimentary load subsidence. This subsidence should have started with a sedimentary thickness of 2.6 km and an antiroot of 12 km. This is the mirror image of the present day crust.

Such a hypothesis can be viewed as excessively simplified. According to what we have just mentioned, the geologic history of the region is very complex and the model presented in this paper might seem to support the rift origin of the Claromecó Basin (Tankard et al. 1996, Pankhurst et al. 2006). Nevertheless results obtained for upper crust are fully consistent with the foreland basin model (Ramos 1984, 2008).

The small crustal attenuation found could be explained also by extensional processes subsequent to the basin foundation, which would have taken place during the Gondwanaland breakup cycle. The modelled Moho geometry is not a clear evidence of the amalgamation of two different thickness crusts in the Tandilia hills as proposed by Ramos (1999b).

CONCLUSIONS

We have prepared a complete local geoid undulations map for the Claromecó intermontane Basin, in order to study its crustal features and isostatic balance. Studying it, together with the Bouguer and magnetic anomalies, we have found that:

(1) The basin is set on a crust with a smooth antiroot, and it is about 12 km thick. Sediments are mainly Paleozoic in age.

(2) Curie isotherm below the Claromecó Basin is lower than below the basin rims, confirming the crustal attenuation beneath the basin.

(3) The basin is isostatically balanced in the Airy system, with a relation 4 to 1 between sedimentary thickness and antiroot height.

(4) From the current model and assuming additional sedimentary load for tectonic stacking as the principal subsidence mechanism, it can be concluded that the sedimentation of the basin could have began with the formation of a graben about 2.6 km thick, and with an antiroot whose thickness could have been about the same as the actual sedimentary thickness.

(5) The top of the basement geometry and deep basement faults were described by using Euler and Werner deconvolutions obtained from gravity and magnetic data.

(6) A simple relationship between local geoid undulations and basement isobaths depths was obtained. This relationship can be used to establish the basin boundaries and sedimentary thickness.

(7) By using a Bouguer anomaly chart together with a local geoid undulations chart the probabilities of obtaining a consistent model are increased. In our model, the calculated sedimentary thickness and Moho depths are consistent with those obtained from the spectral analysis, Euler and Werner deconvolutions.

Acknowledgements

This work was partially supported by grants from the Agencia Nacional de Promoción Científica y Tecnológica and CONICET: "Estudio del margen continental argentino y áreas adyacentes con métodos geopotenciales" (PICTR2002-00166), "Estudio de la evolución futura de cuencas sedimentarias (continuación)" (PIP 03056) and "Tectónica en la Argentina con datos satelitales GOCE" (PICT2007-01903) respectively. CICITCA of Universidad Nacional de San Juan colaborated in this research. Thanks are given to Dr. Pedro Lesta because of his important suggestions and Dr. Marta Ghidella for magnetic data and her suggestions. Dr. Mario E. Gimenez (Universidad Nacional de San Juan) and a further anonymous referee, as reviewers of the journal, helped us in improving the manuscript.

REFERENCES

Andreis R., Iñiguez A., Lluch S. & Rodríguez S., 1989. Cuenca paleozoica de Ventania, Sierras Australes, Provincia de Buenos Aires. *In*: G. Chebli & L.A. Spalletti. (*eds*.): Cuencas Sedimentarias Argentinas. *Serie Correlación Geológica* **6**: 265-298.

Blakely R.J., 1995. Potential theory in gravity and magnetic applications. Cambridge University Press, New York, p. 441.

Brocher T.M., 2005. Empirical Relations between Elastic Wavespeeds and Density in the Earth's Crust. *Bulletin of the Seismological Society of America* **95(6)**: 2081–2092.

Cobbold P., Massabie A. & Rossello E., 1986. Hercynian wrenching and thrusting in the Sierras Australes foldbelt, Argentina. *Hercynica* **II2**: 135-148.

Doint M., Fleiteau L. & McKenzie D., 1996. Geoid anomalies and the estructure of continental and oceanic lithospheres. *Journal Geophysical Research* **101**: 16119-16135.

Du Toit A., 1927. A geological comparison of South America with South Africa. With a paleontological contribution by F. Cowper Reed. *Carnegie Institute of Washington* **381**: 1-158.

Franke D., Neben S., Hinz K., Meyer H. & Schreckenberger B., 2002. Deep crustal structure of the Argentine continental margin from seismic wide-angle and multichannel reflection seismic data. *AAPG Hedberg Conference. Hydrocarbon Habitat of Volcanic Rifted Passive Margins*, p. 4. http://www.searchanddiscovery.net/abstracts/pdf/2002/hedberg_norway/extended/ndx_franke.pdf

Forsberg R., 1985. Gravity Field Terrain Effect Computations by FFT. *Bulletin Geodesique* **59**: 342-360.

Frost B. and Shive P., 1986. Magnetic mineralogy of the lower continental crust. *Journal Geophysical Research* **91**: 6513-6521.

Ghidella M.E., Köhn C. & Gianibelli J.C., 2002. Low Altitude Magnetic Anomaly Compilation in Argentina: its Comparison with Satellite Data. *American Gophysical Union, 2002 Spring Meeting*. .

Gil M., Font G. & Usandivaras J.C., 1995. Modelado de estructuras profundas a partir de datos satelitales. *Actas de las IV Jornadas Geológicas y Geofísicas Bonaerenses* (Buenos Aires) **2**: 117-124.

Guspi F., 1999. Fórmulas compactas para el cálculo del potencial gravitatorio de prismas rectangulares. *In*: Contribuciones a la geodesia en la Argentina de fines del siglo XX. Homenaje a O. Parachú. UNR Editora (Rosario): 129-133.

Guspí F., Introcaso A. & Introcaso B., 2004. Gravity-enhanced representation of measured geoid undulations using equivalent sources. *Geophysical Journal International* **158**: 1-8.

Guspí F., Introcaso A. & Huerta E., 1987. Calculation of gravity effects of three-dimensional structures by analytical integration of a polyhedral approximation and application to the inverse problem. *Geofísica Internacional* **26**: 407-428.

Hartman R.R., Teskey D. J. & Friedberg J.L., 1971. A system for rapid digital aeromagnetic interpretation. *Geophysics* **36**: 891-918.

Haxby W. F. & Turcotte D.L., 1978. On isostatic geoid anomalies. *Journal Geophysical Research* **83**: 5473-5478.

Introcaso A., 2003. Significativa descompensación isostática en la Cuenca del Colorado (República Argentina). *Revista de la Asociación Geológica Argentina* **58(3)**: 474-478.

Introcaso A., 1999. Introducción a la inversión desde las ondulaciones del geoide. *In*: Contribuciones a la geodesia en la Argentina de fines del siglo XX. Homenaje a O. Parachú. U.N.R. Editora (Rosario): 135-164.

Introcaso A., 1993. Predicción del movimiento vertical de una cuenca sedimentaria utilizando el método gravimétrico. *Actas del XII Congreso Geológico Argentino* **1**: 1-4.

Introcaso A., 1982. Resultados gravimétricos sobre las cuencas de la Provincia de Buenos Aires y zonas vecinas. Instituto de Física de Rosario (Rosario): 1-36.

Introcaso A. 1980. A gravimetric interpretation on the Salado Basin (Argentina). *Bolletino di Geofisica Teorica ed Applicatta* (Trieste): **87**: 187-200.

Introcaso A. & Crovetto C., 2005. Introducción a la construcción del geoide. *Temas de Geociencias* **12**: 1-56.

Introcaso A., Guspí F. & Introcaso, B., 2002. Interpretación del estado isostático de la cuenca del Salado (Provincia de Buenos Aires) utilizando un geoide local obtenido mediante fuentes equivalentes a partir de anomalías de Aire Libre. *Actas del XV Congreso Geológico Argentino (El Calafate, Argentina)*. CD-ROM: 1-4.

Introcaso A. & Ramos V., 1984. La cuenca del Salado: un modelo de evolución aulacogénico. *Actas del IX Congreso Geológico Argentino. Tectonofísica en áreas cratónicas móviles* **3**: 27-46.

Jordan T., 1981. Thrust loads and foreland basin evolution, Cretaceus, western Unites States. *American Association of Petroleum Geologists Bulletin* **65**: 2506-2520.

Kostadinoff J. & Prozzi C., 1998. Cuenca de Claromecó. *Revista de la Asociación Geológica Argentina* **53**: 461-468.

Kostadinoff J. & Font G., 1982. Cuenca Interserrana Bonaerense, Argentina. *Actas del V Congreso Latinoamericano de Geología, Buenos Aires* **IV**: 105-121.

Ku C.C. & Sharp J.A., 1983, Werner deconvolution for automated magnetic interpretation and its refinement using Marquart's inverse modeling. *Geophysics* **48(6)**: 754-774.

Lesta P. & Sylwan C., 2005. Cuenca de Claromecó. *Actas del VI Congreso de Exploración y Desarrollo de Hidrocarburos, IAPG (Mar del Plata)*: 217-231.

Limarino C., Massavie A., Rossello E., Lopez-Gamundi O., Page R. & Jalfin G., 1999. El Paleozoico de Ventania, Patagonia e Islas Malvinas. *In*: R. Caminos (*Ed*): Geología Argentina. *Anales del Servicio Geológico Minero Argentino* **29**: 319-348.

López-Gamundi O., Conaghan P., Rossello E. & Cobbold P., 1995. The Tunas Formation (Permian) in the Sierras Australes foldbelt, East-Central Argentina: evidence of syntectonic sedimentation in a Varisican foreland Basin. *Journal of South American Earth Sciences* **8(2)**: 129-142.

López-Gamundi O. & Rosello E., 1992. La cuenca Interserrana de Claromecó, Argentina: un ejemplo de cuenca de antepaís hercínica. *Actas del 8° Congreso Geológico Latinoamericano* **I**: 55-59.

Nabighian M., 1972. The analytic signal of two-dimensional magnetic bodies with polygonal cross-sections: Its properties and use for automated anomaly interpretation. *Geophysics* **37**: 507-517.

Pankhurst R.J., Rapela C.W., Fanning C.M. & Márquez M., 2006. Gondwanide continental collision and the origin of Patagonia. *Earth-Science Reviews* **76**: 235-257.

Pavlis N., Holmes S., Kenyon S. & Factor J., 2008. An Earth Gravitational Model to Degree 2160: EGM2008. *EGU General Assembly 2008 Presentation, European Geosciences Union General Assembly, Vienna, April13-18, 2008*. http://earth-info.nga.mil/GandG/wgs84/gravitymod/egm2008/index.html

Perdomo R. & Del Cogliano D., 1999. The geoid in Buenos Aires region. *International Geoid Service Bulletin (Special Issue for South America)* **9**: 109-116.

Phillips J. D., 1997. Potential-field geophysical software for PC, version 2.2: *U.S.G.S. Open-File Report* **97-725**.

Ploszkiewicz J.V., 1999. ¿Será Buenos Aires una nueva provincia petrolera? Antecedentes, hipótesis y certezas. *Boletin de Informaciones Petroleras, June1999 (Buenos Aires)*: 36-45.

Pucci J.C., 1995. Argentina's Claromecó Basin needs further exploration. *Oil-Gas Journal, September 1995 (Buenos Aires)*: 93-96.

Ramos V., 2008. Patagonia: A paleozoic continent adrift? *Journal of South American Earth Sciences* **26**: 235-251.

Ramos V., 1999a. Las provincias geológicas del territorio argentino. *In*: R. Caminos (*Ed*): Geología Argentina. *Servicio Geológico Minero Argentino, Anales* **29**: 41-96.

Ramos V., 1999b. Rasgos estructurales del territorio argentino. Evolución tectónica de la argentina. *In*: R. Caminos (*Ed*): Geología Argentina. *Servicio Geológico Minero Argentino, Anales* **29**: 715-784.

Ramos V., 1984. Patagonia: un continente a la deriva?. *Actas del IX Congreso Geológico Argentino* **2**: 311-328.

Ramos V.A. & Kostadinoff J., 2005. La cuenca de Claromecó. *In*: R. E. de Barrio, R. O. Etcheverry, M. F. Caballé, E. Llambías (*eds.*), Geología y recursos minerales de la Provincia de Buenos Aires. *Relatorio del 16° Congreso Geológico Argentino*: 473–480.

Rapela C.W., Pankhurst R.J., Casquet C., Fanning C.M., Baldo E.G., González-Casado J.M., Galindo C. & Dahlquist J., 2007. The Río de la Plata craton and the assembly of SW Gondwana. *Earth-Science Reviews* **83**: 49–82.

Rapela C.W., Pankhurst R.J., Fanning C.M. & Grecco L.E., 2003. Basement evolution of the Sierra de la Ventana Fold Belt: new evidence for Cambrian continental rifting along the southern margin of Gondwana. *Journal of the Geological Society (London)* **160**: 613–628.

Reid A., Allsop J., Granser H., Millett A. & Somerton I., 1990. Magnetic interpretation in three dimensions using Euler Deconvolution. *Geophysics* **55**: 80-91.

Ruiz F. & Introcaso A., 2004. Curie point depths beneath Precordillera Cuyana and Sierras Pampeanas obtained from spectral analysis of magnetic anomalies. *Journal Gondwana Research* **8 (4)**: 1133-1142.

Spector A. & Grant F., 1970. Statistical models for interpreting aeromagnetic data. *Geophysics* **35**: 293-302.

Tanaka A., Okubo Y. & Matsubayashi O., 1999. Curie point depth based on spectrum analysis of the magnetic anomaly data in East and Southeast Asia. *Tectonophysics* **306**: 461-470.

Tankard A., Uliana M., Welsink O., Ramos V., Turic M., Franca A., Milani M., De Brito Neves B., Eiles N., Skarmeta J. & Santa-Ana H., 1996. Tectonic controls of basin evolution in southwestern Gondwana. *Petroleum Geologists Memoir* **62**: 5-52.

Thompson D.T., 1982. EULDPH: A new technique for making computer-assisted depth estimates from magnetic data. *Geophysics* **47**: 31-37.

Turcotte D.L. & Schubert G., 2002. Geodinamics (Second Edition). Cambridge University Press, New York, p. 472.

Woollard G.P., 1959. Crustal structure from gravity and seismic measurements. *Journal Geophysical Research* **64**: 1521-1544.

Zambrano J.J., 1974. Cuencas sedimentarias en el subsuelo de la provincia de Buenos Aires y zonas adyacentes. *Revista Asociación Geológica Argentina* **29(4)**: 443-469.